Available online at www.sciencedirect.com
ScienceDirect
Trans. Nonferrous Met. Soc. China 35(2025) 2259−2272
Transactions of Nonferrous Metals Society of China
www.tnmsc.cn

Effect of heat treatment on microstructure and creep behavior of Ti−3.5Al−5Mo−6V−3Cr−2Sn−0.5Fe high-strength β titanium alloy

Jian-kai YANG[1,2], Zhen-quan LIANG[1,2], Shu-long XIAO[1,2], Yun-fei ZHENG[1,2], Xiao-song WANG[1,2], Jing TIAN[1,2], Li-juan XU[1,2]

1. National Key Laboratory for Precision Hot Processing of Metals, Harbin Institute of Technology, Harbin 150001, China;
2. School of Materials Science and Engineering, Harbin Institute of Technology, Harbin 150001, China

Received 19 November 2023; accepted 27 June 2024

Abstract: The effects of heat treatment on microstructure and creep properties of β high-strength titanium alloy, Ti−3.5Al−5Mo−6V−3Cr−2Sn−0.5Fe, were studied. After solution treatment at 790 °C and aging treatment (HT1), the microstructure is composed of equiaxed α_p phase, β phase, α_s phase, and becomes β phase and α_s phases after solution treatment at 840 °C and aging treatment (HT2). The creep behavior at 400 °C was analyzed. The stress exponents of both alloys are between 1 and 2, indicating that the diffusional creep mechanism is one of the dominant creep mechanisms. The alloy after HT2 treatment has better creep resistance and a subsequent creep test on this alloy was performed at 450 °C under 400 MPa. The creep fracture has the mixed ductile−brittle characteristics. The phase interfaces can hinder the dislocation movement, and the α_s phase can coordinate with the matrix to deform, thereby reducing the occurrence of intragranular cracks.

Key words: β high-strength titanium alloy; solution and aging treatment; creep behavior; phase precipitation; α_s phase coarsening

1 Introduction

Titanium alloy has received significant attention and widespread application in the fields of aerospace [1], ocean shipping [2], biomedicine [3], and other fields in recent years due to its excellent mechanical properties, such as low density, high specific strength, and excellent corrosion resistance. With the development of technology, people also need a higher-strength titanium alloy to meet the requirements of some occasions [4,5]. By adjusting the β stable elements in the alloy, β titanium alloy and metastable β titanium alloy can be obtained [6]. They have high strength after appropriate heat treatment. The alloys have a wide range of application prospects and can be used in aircraft landing gear, fasteners, and other parts [7,8]. Heat treatment can significantly affect the microstructure and mechanical properties of β titanium alloys [9,10]. ZHU et al [11] found that the heat treatment improved the microscopic structure of the laser additive manufacturing TC17 alloy and let its mechanical properties close to the aviation standard for TC17. WANG et al [12] found that the microstructure of TC21 alloy evolved with different heat treatment regimes. ELSHAER and IBRAHIM [13] investigated the relationship among the microstructure, deformation behavior, and mechanical properties of TC21 alloy after solution

Corresponding author: Shu-long XIAO, Tel: +86-18745796616, E-mail: xiaoshulong@hit.edu.cn;
Li-juan XU, Tel: +86-18845618175, E-mail: xljuan@hit.edu.cn
https://doi.org/10.1016/S1003-6326(25)66813-0

and aging treatments. When aging treatment in the two-phase region, the fine secondary α phases (α_s) precipitate from the β matrix, which significantly improves the performance of the alloy. WU and ZHAN [14] studied the Ti-55531 near-β titanium alloy and found that during the aging treatment, the coarsening of the α_s phase occurred, and the coarsened α_s phases increased the crack propagation resistance and finally improved the toughness of the alloy.

Considering the application environment of the alloy, it is required that the high-strength titanium alloys not only have good mechanical properties but also have a long service life, so there should be certain requirements for the creep properties of the alloy. Studies have shown that heat treatment has a significant effect on the creep properties of the alloy [15,16]. KIM et al [17] found that the selective laser melting Ti−6Al−4V alloy had relatively low creep strain and low steady-state creep rate after heat treatment. NIE et al [18] performed different heat treatments on the Ti−5Al−5Mo−5V−1Fe−1Cr alloy and obtained the equiaxed structure and lamellar structure, and finally found that the creep resistance of the lamellar structure was better than that of equiaxed structure. XIAO et al [19] studied the effects of heat treatment on the microstructure and creep properties of TC4 alloy and found that heat treatment significantly improved the creep life of the alloy. YU et al [20] studied the creep behavior of Ti−15V−3Cr−3Al−3Sn β titanium alloys and found that pre-aging materials had better creep properties than dynamic aging materials because of the further increase of prior β grain size, lamellar α volume fraction, and lamellar α length in pre-aging creep. WANG et al [21] studied the Ti−5.8Al−3Sn−5Zr−0.5Mo−1Nb−1Ta−0.4Si−0.2Er alloy and found that after the designed hot working and heat treatment, a triple-microstructure with the participation of silicide appeared in the alloy. This structure was formed along the α_2 phase and phase interface can effectively improve thermal stability and creep resistance.

Previous studies have shown that as a self-developed metastable β titanium alloy, Ti−3.5Al−5Mo−6V−3Cr−2Sn−0.5Fe has excellent mechanical properties [22,23]. Considering that the alloy should have a long service life, it is necessary to further study the creep properties of the alloy. In this work, the rolled Ti−3.5Al−5Mo−6V−3Cr−2Sn−0.5Fe alloy was solution-treated in the two-phase region and single-phase region, respectively, and then aging treatment, and the effect of heat treatment on the microstructure evolution and creep properties of the alloy was studied.

2 Experimental

2.1 Material preparation and heat treatment

The Ti−3.5Al−5Mo−6V−3Cr−2Sn−0.5Fe alloy was prepared by vacuum consumable arc melting technology. The α/β phase transition temperature of the alloy was determined in the range of (815±5) °C. The forging process of the alloy is shown in Fig. 1(a) and the forging process is as follows. Before the start of forging, the surface defect parts were removed first, and then five forging treatments were carried out to ensure a uniform internal structure. After heating to 980 °C for 2 h, the first forging treatment was carried out. The sample was heated to 870 °C for 100 min for the second forging treatment, and then heated to 780 °C for 90 min for the last three forging treatments to obtain the forged alloy [22,23]. The alloy was further rolled at 790 °C in the (α+β) two-phase region with a deformation of 40%.

Solution and aging treatments of the rolled alloy were carried out in the resistance furnace and the heat treatment scheme is shown in Fig. 1(b), which was named HT1 (solution treatment at 790 °C + aging treatment at 560 °C) and HT2 (solution treatment at 840 °C + aging treatment at 560 °C), respectively. The samples were pre-coated with anti-oxidation coating and the oxide layer was removed after heat treatment.

2.2 Creep test

The alloy was made into creep samples with the dimensions shown in Fig. 2(a), and the creep samples were made along the rolling direction of the alloy. Creep tests were conducted on the RDL100 creep testing machine at 400 °C under 200, 300, and 400 MPa, respectively. Before the test, the creep samples were treated with 240−2000 mesh sandpapers in order to obtain sufficient surface finish and avoid the impact of surface processing scratches on the test results. Subsequently, the alloy with better creep resistance was selected for the creep test at 450 °C under 400 MPa. During the creep tests, three thermocouples were used to

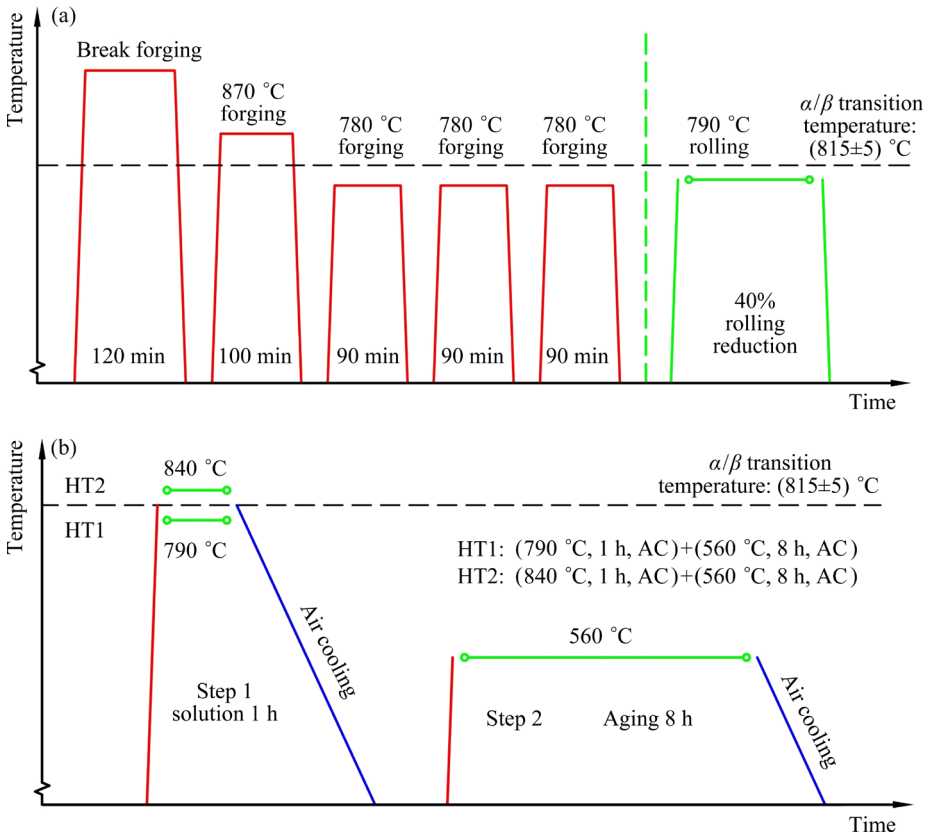

Fig. 1 Schematic descriptions of hot working process (a) and heat treatment routes (b) of alloy

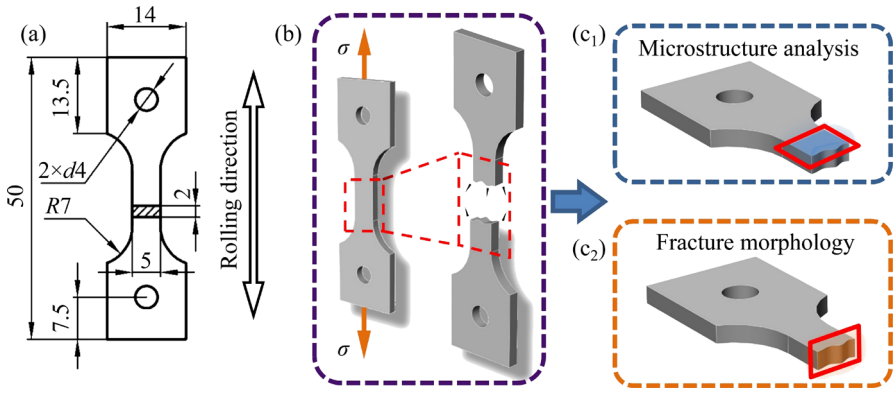

Fig. 2 Schematic diagram related to creep samples: (a) Size of creep sample (in mm); (b) Drawing direction and fracture position of creep sample; (c_1) Location for microstructural observation; (c_2) Observation position for fracture morphology

measure the temperature of the upper and lower gripping heads and the gauge section of the sample, respectively, to ensure temperature stability during the test. The upper rod was fixed, and the creep deformation of the sample is obtained by detecting the displacement of the lower rod.

2.3 Microstructure characterization

X-ray diffraction (XRD) analysis (Empyrean machine) was performed on the samples after heat treatment. Scanning electron microscopy (SEM, Quanta 200FEG) was used to observe the phase structure, the fracture morphology, and the microstructure near the fracture in secondary electrons mode (SE). The microstructure near the fracture was also analyzed by transmission electron microscopy (TEM, Talos F200X). The selected positions are shown in Figs. 2(c_1, c_2). Samples used for SEM analysis were ground with sandpapers of 240−2000 mesh and then mechanically polished.

Samples for TEM analysis were first ground to a thickness of 50 μm and then prepared by argon ion beam thinning techniques.

3 Results and discussion

3.1 Microstructure after heat treatment

Figure 3 shows the XRD patterns of the alloy after different heat treatments. After heat treatment, the alloy is mainly composed of α phase and β phase, and there are no other phase components. Strong diffraction peaks of α and β phases appear in the alloy after HT1 simultaneously. Compared with the alloy after HT2, the alloy after HT1 has stronger α diffraction. According to the normalized strength theory [24], the stronger diffraction peak corresponds to more α phases in the microstructure.

The microstructure of the alloy after HT1 treatment is shown in Figs. 4(a−c). The microstructure of the alloy is composed of β phase, primary α phase (α_p), and α_s phase. The α_p phases are mainly equiaxed α phases, rod-like α phases and continuously distributed grain boundary α phases (α_{GB}), as shown in Fig. 4(b). It can be seen from Fig. 4(a) that some α_p phases are distributed in bands or strips along the rolling direction, while from Fig. 4(b), these banded structures are actually composed of many equiaxed α_p or rod-like α_p phases. The rolling is completed at the temperature

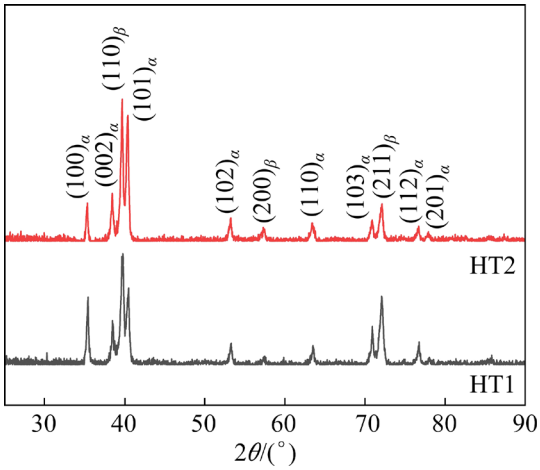

Fig. 3 XRD patterns of alloy after different heat treatments

of the two-phase region, and the α_p phases are broken and elongated during the rolling process, which are distributed in bands or strips along the force direction. In the subsequent heat treatment process, these broken α phases can be used as the nucleation points of the α_p phase precipitated in the solution treatment process, forming the belt aggregation distribution of the equiaxed α phases. This structure makes the alloy properties anisotropic, and the performance in the direction parallel to the strip structure is better than that in the direction perpendicular to the strip structure.

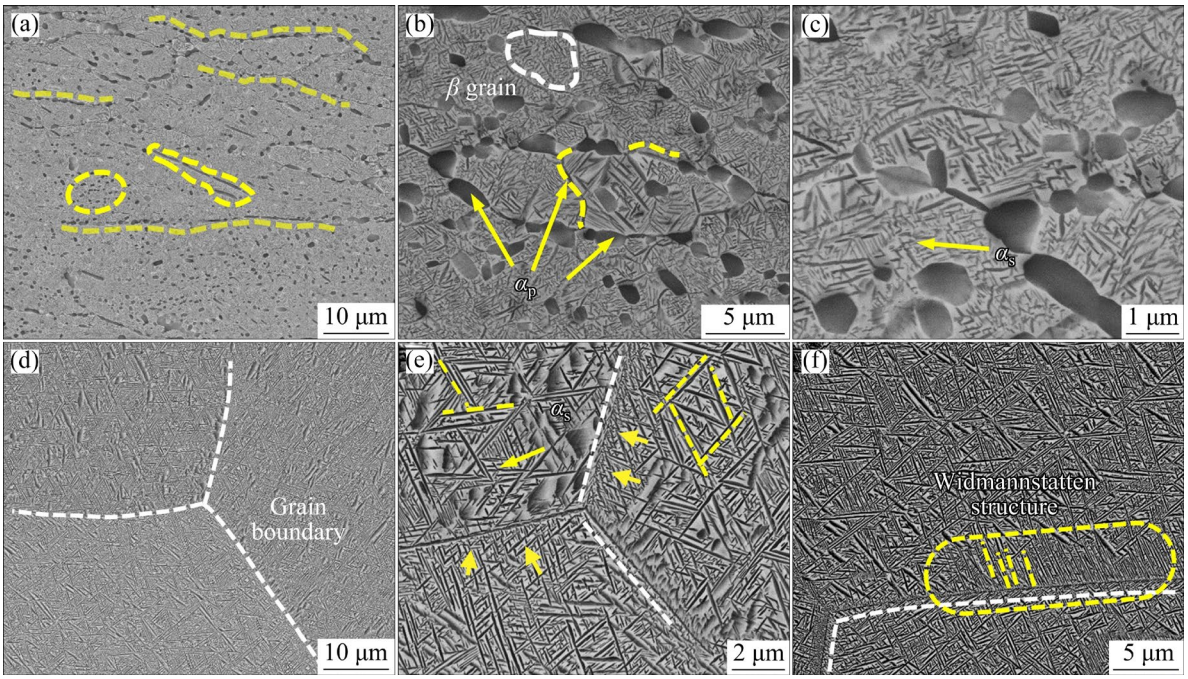

Fig. 4 Microstructure of alloy after different heat treatments: (a−c) HT1; (d−f) HT2

In addition, due to the dislocations and grain fragmentation generated by rolling, the number of nucleation points of α_p phase and β phase increases, and the nucleation capacity is enhanced. At the same time, many α_p phases hinder the growth of β grains, so the final β grain size is very small, only a few microns. There are many contiguous α_{GB} phases. The α_s phase is needle-like precipitate, generally less than 1 μm, and it uniformly disperses and precipitates on the β matrix. It can be seen that a large number of α_p phases spheroidize obviously, making the interface no longer continuous. This reduces the aspect ratio, and the effective distance of crack propagation along the grain boundary can be shortened to a certain extent.

The microstructure of the alloy after HT2 treatment is shown in Figs. 4(d−f). The alloy is composed of β phase and lamellar α_s phase, with the α_p phase disappearing during the solution treatment process in the single-phase region. The β phase recrystallizes into equiaxed grain, and no obvious traces of rolling can be seen. The size of the β grain is significantly larger than that of the alloy after HT1. The typical trigeminal grain boundaries of the β titanium alloy can be seen in Fig. 4(d). Parallel packets of α appear at the grain boundaries, which are called the Widmannstatten structure (hereinafter referred to as "*W* phase"). Studies have shown that the α_{GB} phase can be the parent phase of this kind of microstructure, which has high strength and can hinder crack propagation through the grain boundary, reducing the plasticity of the alloy [25,26]. The size of the lamellar α_s phase can reach up to 3−5 μm. The α_s phases precipitated in the later stage nucleate and grow in the skeleton composed of the α_s phase precipitated in the early stage, and the growth space is smaller, so the size is smaller. It can be seen that there is a certain angular relationship among the α_s phases, indicating that there is a certain relationship between the α_s phase and the β matrix.

3.2 Creep behavior of alloy at 400 °C

The results of the creep tests performed on the Ti−3.5Al−5Mo−6V−3Cr−2Sn−0.5Fe alloy after different heat treatments under different stresses at 400 °C are shown in Fig. 5 and Table 1. All of the tests are stopped at 20 h, and no samples are broken at the end of the tests. It can be seen from Fig. 5 that the creep curves of all the samples only show the primary creep stage and the steady-state creep stage. In the primary creep stage, the creep strain of the alloy increases rapidly. The plastic deformation occurs continuously in the alloy, resulting in lots of dislocations. The strain hardening effect appears in the alloy, which makes the increasing rate of creep strain gradually slow down. But overall the strain is still increased, which also causes the strain-hardening effect to continue to increase. When the strain hardening caused by long-range dislocation

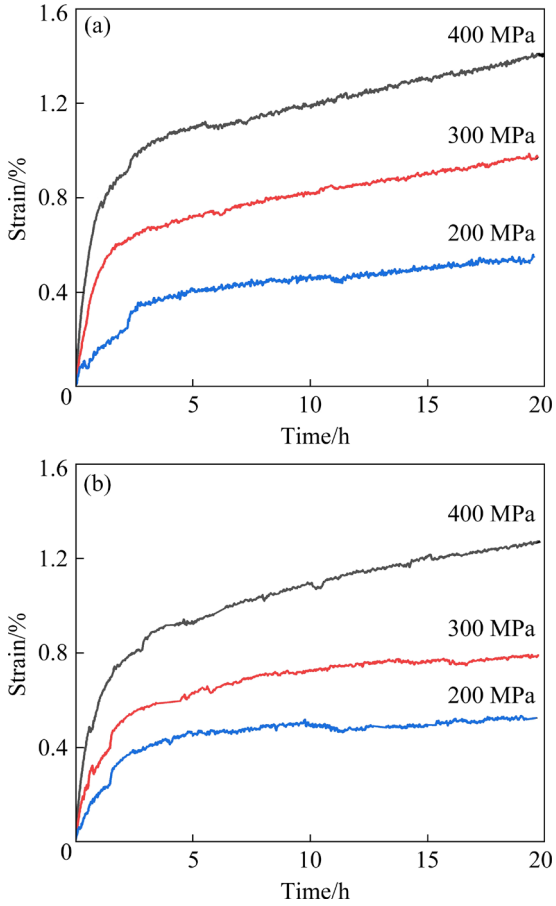

Fig. 5 Creep curves of alloy tested at 400 °C under different stresses in air: (a) HT1; (b) HT2

Table 1 Creep strain and steady-state creep rate of alloy tested at 400 °C under different stresses in air

Heat treatment	Temperature/°C	Stress/MPa	Creep strain/%	Steady-state creep rate/s^{-1}
HT1	400	200	0.56	2.35×10^{-6}
		300	0.99	3.99×10^{-6}
		400	1.41	6.59×10^{-6}
HT2	400	200	0.53	1.53×10^{-6}
		300	0.79	2.02×10^{-6}
		400	1.27	4.40×10^{-6}

interaction is continuously enhanced and can achieve the dynamic equilibrium with the strain recovery caused by the thermal activation of short-range dislocation movement, the creep of the alloy enters the steady-state creep stage. As seen from Table 1, for the alloy after HT1, when tested at 400 °C, the creep strain is 0.56% at 200 MPa, 0.99% at 300 MPa, and 1.41% at 400 MPa. For the alloy after HT2, the creep strain is 0.53% at 200 MPa, 0.79% at 300 MPa, and 1.27% at 400 MPa, which are all smaller than the creep strain of the alloy after HT1 under the same conditions. This shows that with the creep stress increasing, the creep strain of the alloy increases, the creep phenomenon becomes more obvious, and the alloy after HT2 treatment has better creep resistance than the alloy after HT1.

For the three stages of the creep process in most titanium alloys, the steady-state stage accounts for most of the process, so it is necessary to focus on the steady-state creep mechanism of the alloy. The creep rate of the steady-state creep stage of the alloy is calculated and the result is given in Table 1. It can be seen that with the increase of creep stress, the steady-state creep rate of the alloy gradually increases, and the steady-state creep rate of the alloy after HT2 treatment is generally lower than that of the alloy after HT1 treatment under the same conditions.

It is necessary to obtain the creep stress exponent (n) to get the creep mechanism. The relationship between the steady-state creep strain rate and the creep stress is usually expressed by the Norton−Bailey equation [27,28]:

$$\dot{\varepsilon}_s = A\sigma^n \exp\left(-\frac{Q_c}{RT}\right) \tag{1}$$

where $\dot{\varepsilon}_s$ is the steady-state strain rate (s^{-1}), A is the material constant; σ is the experimental stress (MPa); n is the stress exponent; Q_c is the creep activation energy (kJ/mol); R is the molar gas constant; T is the temperature (K). From Eq. (1), the expression of the stress exponent (n) is

$$n = \left(\frac{\partial \ln \dot{\varepsilon}_s}{\partial \ln \sigma}\right)_T \tag{2}$$

The difference in stress exponent (n) indicates different creep mechanisms. Figure 6 shows the linear fitting result of the steady-state creep rate and creep stress of the alloy, and the slope of the linear fitting curve is the stress exponent (n). When the creep temperature is 400 °C, the stress exponent (n) of the alloy after HT1 is 1.48, and the stress exponent (n) of the alloy after HT2 is 1.47. Both are between 1 and 2, so the diffusional creep mechanism is one of the creep mechanisms [29].

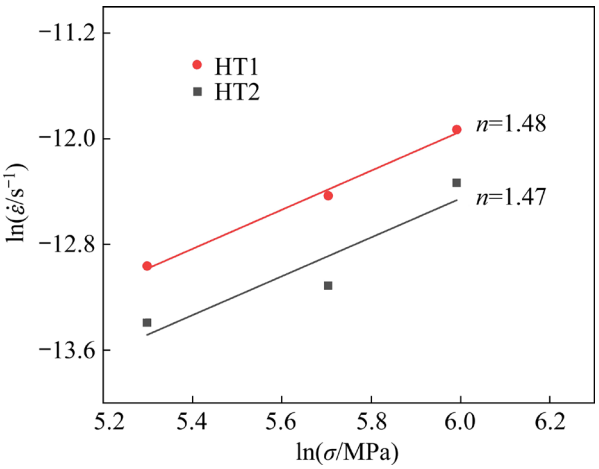

Fig. 6 Double natural logarithmic plots of steady-state creep rate versus stress of alloy

3.3 Evolution of microstructure during creep at 400 °C

Figure 7 shows the microstructure of the deformation region after creep. The temperature of the creep test is in the temperature range of the aging treatment of the alloy. At this time, the aging process of the alloy continues under the dual action of temperature and stress, and as stress increases, the aging process of the alloy becomes more obvious [20]. Studies have shown that during the aging process, with the extension of time, the α_s phase in the β titanium alloy is coarsened, and the volume fraction of the α_s phase in the alloy increases [25,30]. Therefore, during creep, due to the aging process, the α_s phases grow further on the basis of the original α_s phases or form nuclei and grow up at the positions with more defects such as dislocations. For the alloy after HT1, as shown in Fig. 7(a), there are still many fine α_s phases after creeping at 200 MPa, and the growth of the α_s phase is not obvious yet. The slipping length for dislocations of these fine α_s phases is smaller, which minimizes the creep strain of the alloy [31]. With the increase of the creep stress, the aging process becomes more obvious, and the coarsening degree of α_s phase increases. More large-size α_s phases

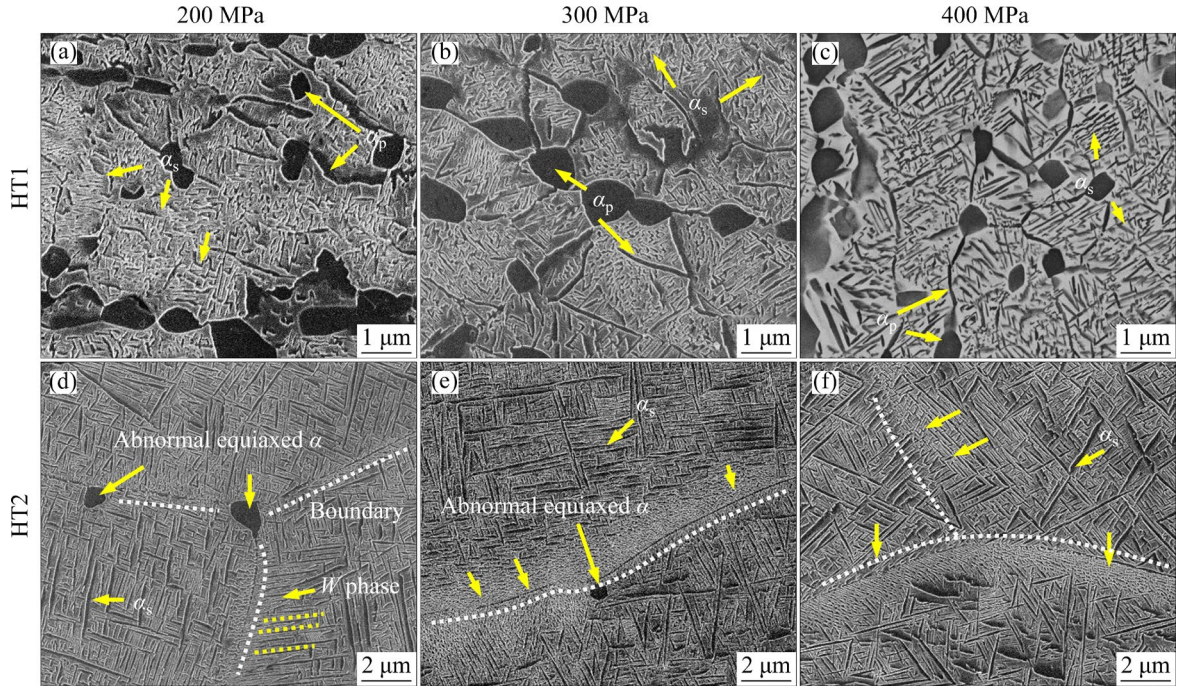

Fig. 7 Microstructures of deformation region after creep tests at 400 °C under different stresses in air

appear, which indicates that creep stress affects the microstructure evolution of the alloy during creep, and the greater the creep stress, the larger the α_s phase size, so the alloy shows worse creep performance and more obvious creep deformation.

For the alloy after HT2, the trends of the α_s phases within the grain and near the grain boundary are different. After creep, under the action of dynamic aging, in the grain interior, the α_s phases tend to grow on the basis of the original α_s phases. Near the grain boundary, a number of fine α_s phases precipitate due to more defects such as dislocation pile-ups, which is easier for the nucleation of the α_s phase. Unlike the Widmannstatten structure (the "*W* phase" in Fig. 7), which increases the brittleness, these fine α_s phases can make a significant strengthening effect and increase the resistance of dislocation movement. Although the solution treatment of the alloy is in the single-phase region and there is no equiaxed α phase in the original structure, abnormal equiaxed α phases precipitate at the alloy grain boundary after creep. A similar phenomenon was also reported by CHEN et al [32], which is caused by the diffusion of β stable elements such as Mo in the alloy to the grain boundary, and the reverse movement of α stable elements such as Al. The abnormal equiaxed α phases reduce the performance of the alloy. With the creep stress increasing, the amount of precipitation of these abnormal equiaxed α phase decreases, as the higher stresses make it easier for atoms to reach the diffusion activation energy, making it difficult for α stable elements to aggregate in a single region.

In general, the soft α phases precipitated on the grain boundaries preferentially undergo creep deformation [33]. By comparing the microstructure of the alloy before and after creep, it can be known that compared with the alloy after HT2 treatment, the alloy after HT1 treatment has a smaller grain size and a large amount of equiaxed α phases and incoherent α/β interfaces. On the one hand, this microstructure makes the alloy after HT1 treatment more conducive to the diffusion of atoms and vacancies than the alloy after HT2 treatment, and the participation of grain boundary sliding and deformation of the soft α phase make the creep process of the alloy after HT1 deform greatly. On the other hand, there is a certain orientation relationship between the acicular α_s phase and the β phase in the alloy after HT2 treatment, which provides lots of semi-coherent phase interfaces with lower diffusion rates and dislocation creep rates [18]. The combination of these factors makes the alloy after HT2 treatment have better creep resistance.

3.4 Creep behavior of alloy after HT2 treatment at 450 °C

The above results show that the rolled alloy after HT2 (solution treatment in the β single phase region + aging treatment) has better creep resistance, so the creep test at 450 °C and 400 MPa was further carried out, and the results are shown in Fig. 8. It can be seen that this creep test also shows the primary creep stage and the steady-state creep stage, and the sample is fractured in the steady-state creep stage. Finally, the creep strain of the alloy is 8.27%, the creep life of the alloy is 113.1 h, and the steady-state creep rate of the alloy increases to 1.07×10^{-5} s^{-1}.

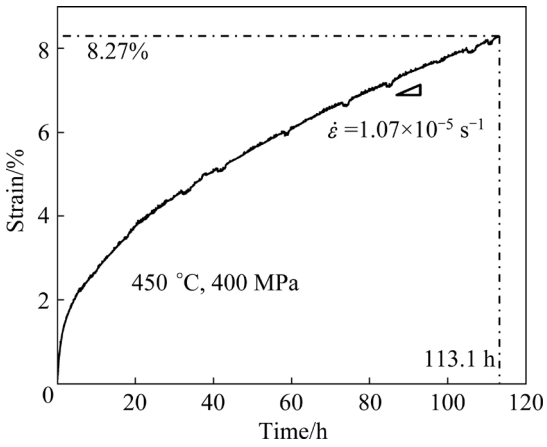

Fig. 8 Creep curve and corresponding creep data of alloy after HT2 heat treatment tested at 450 °C under 400 MPa in air

3.5 Microstructure and fracture after creep at 450 °C

Figure 9 shows the microstructure of the deformation area near the fracture after the creep test of the Ti−3.5Al−5Mo−6V−3Cr−2Sn−0.5Fe alloy at 450 °C under 400 MPa in air. As can be seen in Figs. 9(a, b), many cracks are initiated at the grain boundaries and grow further along the grain boundaries. There are significant cracks among the grains. These cracks grow along β grain boundaries and penetrate deeply into the alloy, which is one of

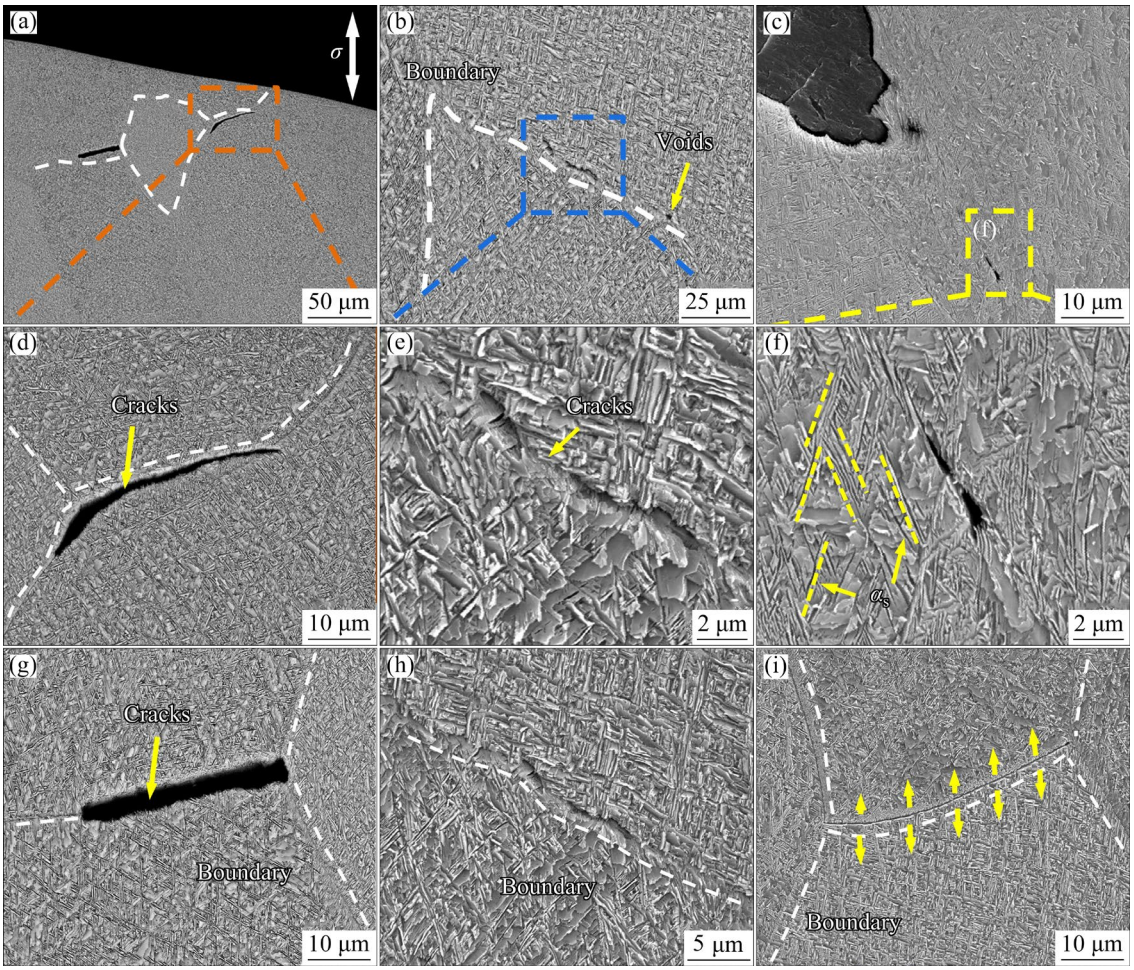

Fig. 9 Microstructures near fracture of HT2 alloy after creep test at 450 °C under 400 MPa in air

the direct reasons of alloy fracture. And as seen from Fig. 9(f), cracks also appear in alloy grains, but are in small quantities and mainly distributed at the phase interfaces. The growth direction of the cracks in the grains is blocked by the intricate α_s phases, so it is difficult to grow further.

Figure 10 shows the fracture morphology of the alloy after the creep test at 450 °C under 400 MPa. Obvious cleavage fracture features and intergranular fracture features can be seen, as shown by the large amounts of river patterns in Fig. 10(a) and the large amounts of small-plane structures in Fig. 10(d). There are also many dimples on the fracture, as shown in Figs. 10(c, e). On the whole, the fracture mode of the alloy belongs to the mixed ductile−brittle fracture characteristics, which is also consistent with the characteristics of the creep curve terminating in the steady-state creep stage, indicating that the alloy fractures abruptly during the creep process.

Figure 11 shows the elaborate TEM characterization of HT2 alloy after the creep test at 450 °C under 400 MPa in air. From Figs. 11(a−c), there are many dislocations in the α_s phases and the β phases. During the creep process, there are lots of α_s phases in the grains, which on the one hand provide a smaller slipping length for dislocations, and on the other hand, play a good role in the precipitation strengthening effect. The large number of phase interfaces formed by the α_s phases and the β phases can hinder the sliding of dislocations. As shown in Fig. 11(d), large amounts of dislocations are plugged at the phase interfaces. Therefore, the α_s phase improves the creep resistance of the alloy. In Fig. 9(f), it can be also seen that the α_s phases are significantly deflected under the action of stress, which tends to be distributed along the stress direction, and the orientation angle between the α_s phases is significantly reduced compared with that before the creep. This indicates that the α_s phase and the β phase in the grain are harmoniously deformed. After HT2 treatment, the alloy has high creep resistance and still has good compatible deformation ability.

The orientation relationship between the α_s phase and the β phase of the alloy was analyzed, and the results are shown in Figs. 11(e_1−e_4). According to the Fourier transform of the high-resolution lattice image, it can be seen that the upper part in Fig. 11(e) is composed the β phase and the lower part is composed of the α phase. It can be further concluded from Figs. 11(e_3, e_4) that the orientation relationship between the α_s phase and the β phase is $[\bar{1}100]_\alpha // [111]_\beta$ and $(0002)_\alpha // (01\bar{1})_\beta$. So, the α_s phase and β phase are strictly in accordance with the Burgers orientation relationship: $\langle 11\bar{2}0\rangle\{0001\}_\alpha // \langle 111\rangle\{110\}_\beta$ [34]. The phase interface of the α_s phase and the β phase is semi-coherent, where a large number of dislocations are evenly distributed, as shown in the

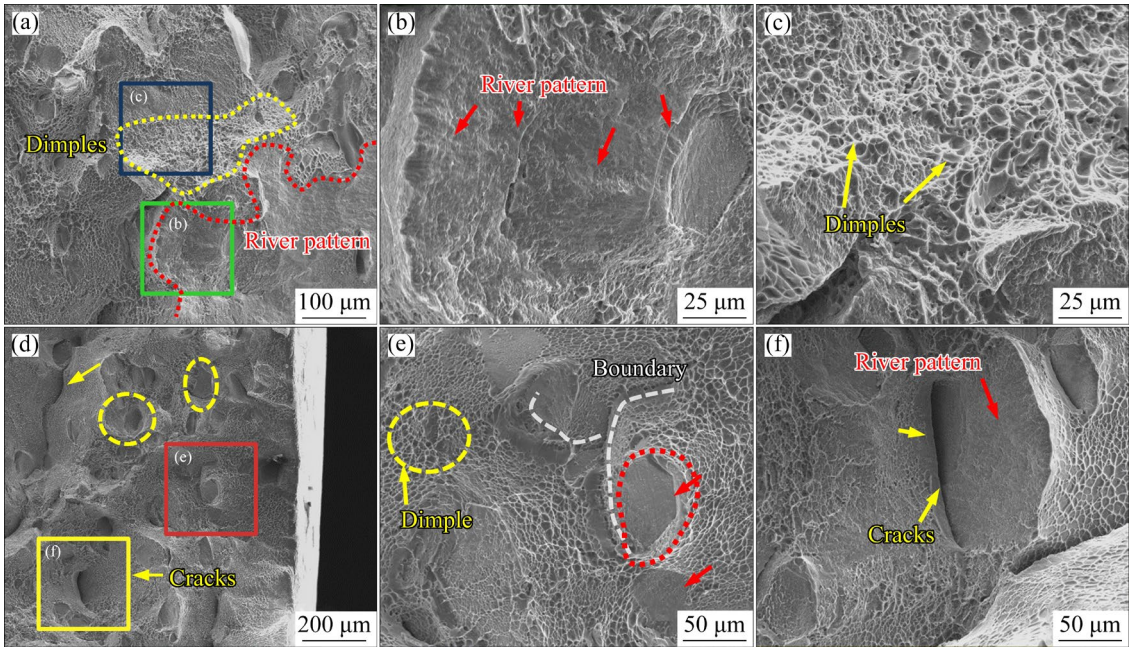

Fig. 10 Creep fracture morphologies of HT2 alloy after creep test at 450 °C under 400 MPa in air

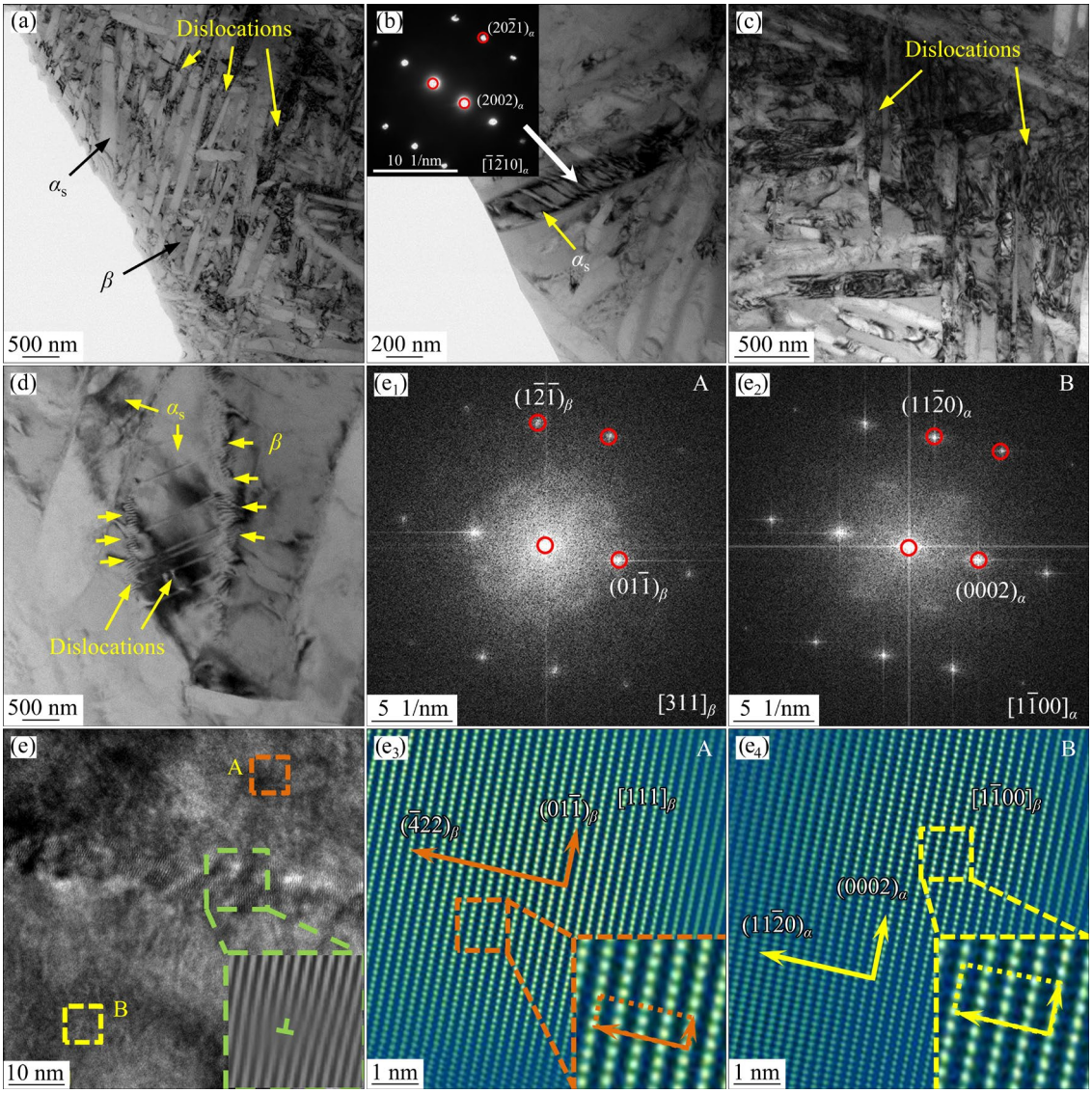

Fig. 11 TEM characterization of HT2 alloy after creep test at 450 °C under 400 MPa in air: (a) Morphology of β matrix and α_s phase; (b) Dislocations and diffraction pattern of α_s phase; (c) Dislocations distribution; (d) Phase interfaces; (e) High-resolution transmission electron microscope (HRTEM) image and inverse fast Fourier transform (IFFT) image about phase interface; (e_1) Selected area electron diffraction (SAED) pattern of Region A; (e_2) SAED pattern of Region B; (e_3) IFFT image of Region A; (e_4) IFFT image of Region B

lower right corner of Fig. 11(e). Compared with the large number of incoherent grain boundaries in the alloy after HT1, this semi-coherent interface has weak diffusion capabilities and dislocation sliding ability, and the vacancy diffusion rate is also low, which can effectively improve the creep resistance. Therefore, there are many dislocation pile-ups at the phase interfaces, as shown in Fig. 11(d).

The aging process continues during the creep process. The original α_s phases are generally coarsened and deflected under stress. This evolution of the precipitated phase is one of the manifestations of diffusion creep [35]. It can be seen in Fig. 9 that cracks are more likely to occur at the grain boundary, and the grain boundary undergoes a certain degree of deformation. Especially in Fig. 9(i), some grain boundaries have the tendency to be pulled apart along the direction of stress, which shows that the grain boundary sliding is involved in the creep process, but this is not the main mechanism. It can be seen from Fig. 11 that dislocations appear, and are hindered by the phase interfaces and the grain boundaries, forming a large number of dislocation pile-ups.

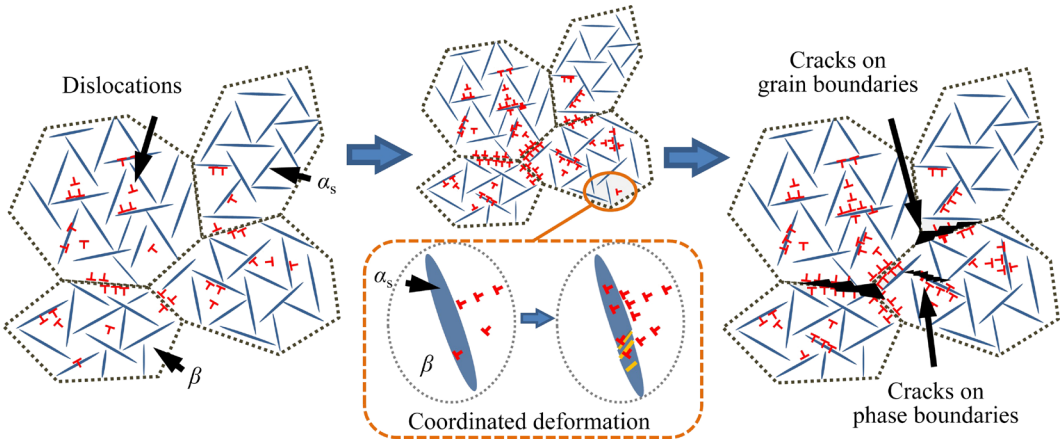

Fig. 12 Schematic diagram of alloy fracture process during creep

There are also straight dislocation lines in the α phases and the adjacent β phases, but the number is limited, and the movement space is limited by the extremely small precipitated phases, so the dislocation slipping is limited. In summary, the diffusional creep mechanism is still one of the dominant creep mechanisms at 450 °C, and at the same time, the grain boundary sliding mechanism and dislocation slipping mechanism are also involved.

3.6 Fracture mechanism

The mechanism of the Ti−3.5Al−5Mo−6V−3Cr−2Sn−0.5Fe alloy creep fracture is shown in Fig. 12. With the deformation beginning, many dislocations are generated in the grains. The dislocations continue to slip. Both the phase boundary and the grain boundary can hinder the movement of the dislocations, resulting in the formation of dislocation pile-ups at the boundaries, further causing stress concentrations. When the creep deformation is further carried out and until the stress concentrations caused by the dislocation pile-ups are greater than the strength of interface, cracks appear in both the phase boundary and the grain boundary. However, when the dislocation pile-ups at the phase interfaces reach a certain extent, the dislocations generated in the α_s phases and the β phases can grow forward through the semi-coherent interface, and the α_s phases and β matrix can be deformed in coordination, which can reduce the stress concentration and thus reduce the number of the cracks. At the same time, with temperature increasing, the grain boundaries begin to exhibit weak viscosity, which reduces the strength of the grain boundaries and makes the grain boundaries become the weakened regions. As a result, finally, there are fewer cracks at the phase boundaries, and the growth of the cracks at the phase boundaries can be hindered by the staggered α_s phases within the grain, while cracks are more likely to occur at the grain boundaries. After HT2 heat treatment, the grain size is large and the grain boundary is relatively straight. There is no other phase or structure to hinder the growth of the cracks when they grow along the grain boundaries, so it is easy for the micropores and cracks to grow along the grain boundary, resulting in the characteristics of intergranular fracture. The cracks on the grain boundaries further reduce the bearing area of the alloy, so that eventually the cracks are enough to pass through the remaining grains, causing the alloy to fracture.

4 Conclusions

(1) Before the creep, the microstructure of the alloy after solution treatment in the α+β two-phase region and aging treatment (HT1) is composed of equiaxed α_p phase, β phase, and lamellar α_s phase. The microstructure of the alloy after solution treatment in the β single-phase region and aging treatment (HT2) is composed of β phase and lamellar α_s phase.

(2) After the creep tests at 400 °C, the creep curves show the primary stage and the steady-state stage. The diffusional creep mechanism is one of the creep mechanisms. Benefiting from the fewer grain boundaries and more semi-coherent phase boundaries, the creep strain and steady-state creep

rate of the alloy after HT2 heat treatment are smaller, so the alloy after HT2 heat treatment has better creep resistance.

(3) After creep, the α_s phase in the alloy after HT1 heat treatment is coarsened, and the coarsening effect becomes more obvious with the increase of stress. The α_s phase of the alloy after HT2 heat treatment shows obvious refinement near the grain boundary, and the equiaxed α phases abnormally precipitate after creep.

(4) After creeping at 450 °C, the fracture of the alloy after HT2 has the mixed ductile−brittle characteristics. The semi-coherent phase interface can effectively improve the creep resistance. The β phase and α_s phase can be deformed harmoniously. In addition, crack propagation at the phase interface is limited by the staggered α_s phases. So, more cracks grow at the grain boundaries, eventually along with the cracks on the phase boundaries, causing the alloy to break.

CRediT authorship contribution statement

Jian-kai YANG: Investigations, Formal analysis, Data curation, Writing − Original draft; **Zhen-quan LIANG:** Software, Writing − Reviewing & editing; **Shu-long XIAO:** Data curation, Writing − Reviewing & editing; **Yun-fei ZHENG:** Methodology, Writing − Reviewing & editing; **Xiao-song WANG:** Data curation; **Jing TIAN:** Visualization; **Li-juan XU:** Resources, Supervision.

Declaration of competing interest

The authors declare that they have no known competing financial interests or personal relationships that could have appeared to influence the work reported in this paper.

Acknowledgments

This work was supported by the National Natural Science Foundation of China (No. 51975147).

References

[1] WU Yong, FAN Rong-lei, QIN Zhong-huan, CHEN Ming-he. Shape controlling and property optimization of TA32 titanium alloy thin-walled part prepared by hot forming [J]. Transactions of Nonferrous Metals Society of China, 2021, 31: 2336−2357. https://doi.org/10.1016/S1003-6326(21)65658-3.

[2] LI Yang, ZHOU Ze-long, YI Xue-ning, YAN Ji-wen, XIU Jun-jie, FANG Da-zhen, SHAO Ming-hao, REN Ping, HE Yong-yong, QIU Jian-xun. Improved seawater corrosion resistance of electron beam melting Ti6Al4V titanium alloy by plasma nitriding [J]. Vacuum, 2023, 216: 112463. https://doi.org/10.1016/j.vacuum.2023.112463.

[3] HAZWANI M R S N, LIM L, LOCKMAN Z, ZUHAILAWATI H. Fabrication of titanium-based alloys with bioactive surface oxide layer as biomedical implants: Opportunity and challenges [J]. Transactions of Nonferrous Metals Society of China, 2022, 32: 1−44. https://doi.org/10.1016/S1003-6326(21)65776-X.

[4] GUO Zhen-guo, MA Tie-jun, YANG Xia-wei, LI Wen-ya, TAO Jun, LI Ju, VAIRIS A. Thermo-physical simulation of deformation behavior and microstructure evolution for linear friction welding of near-β titanium alloy [J]. Transactions of Nonferrous Metals Society of China, 2023, 33: 481−493. https://doi.org/10.1016/S1003-6326(22)66121-1.

[5] ZHANG Chang-jiang, JIANG Xi, LÜ Zhi-dan, FENG Hong, ZHANG Shu-zhi, XU Ying, HAYAT M D, CAO Peng. Effect of duplex aging on microstructure and mechanical properties of near-β titanium alloy processed by isothermal multidirectional forging [J]. Transactions of Nonferrous Metals Society of China, 2022, 32: 1159−1168. https://doi.org/10.1016/S1003-6326(22)65863-1.

[6] HUANG Liang, LI Chang-min, LI Cheng-lin, HUI Song-xiao, YU Yang, ZHAO Ming-jie, GUO Shi-qi, LI Jian-jun. Research progress on microstructure evolution and hot processing maps of high strength β titanium alloys during hot deformation [J]. Transactions of Nonferrous Metals Society of China, 2022, 32: 3835−3859. https://doi.org/10.1016/S1003-6326(22)66062-X.

[7] LI Chao-hua, CUI Yi-min, ZHENG Wei-wei, SONG Lin, WU Yu-lun, WU Yi-dong, YU Chun-yan, HUI Xi-dong. Unveiling the dynamic softening mechanism via micromechanical behavior for a near-b titanium alloy deformed at a high strain rate [J]. Journal of Materials Research and Technology, 2023, 26: 9392−9405. https://doi.org/10.1016/j.jmrt.2023.09.150.

[8] MANIKANDAN P, KUMAR K N, RAO G S, JHA A K, NARAYANAN P R, PANT B, CHENRIAN R M. Fracture toughness of Ti−15V−3Cr−3Sn−3Al titanium alloy in different heat-treated conditions [J]. Transactions of the Indian Institute of Metals, 2019, 72(6): 1507−1510. https://doi.org/10.1007/s12666-019-01572-9.

[9] WANG Zhen-yu, LIU Li-bin, WU Di, ZHANG Li-gang, WANG Wan-lin, ZHOU Ke-chao. α'' phase-assisted nucleation to obtain ultrafine α precipitates for designing high-strength near-β titanium alloys [J]. Transactions of Nonferrous Metals Society of China, 2020, 30: 2681− 2696. https://doi.org/10.1016/S1003-6326(20)65412-7.

[10] XU Sheng-hang, LIU Yong, LIU Bin, WANG Xin, CHEN Zhi-xin. Microstructural evolution and mechanical properties of Ti−5Al−5Mo−5V−3Cr alloy by heat treatment with continuous temperature gradient [J]. Transactions of Nonferrous Metals Society of China, 2018, 28: 273−281. https://doi.org/10.1016/S1003-6326(18)64660-6.

[11] ZHU Yan-yan, CHEN Bo, TANG Hai-bo, CHENG Xu, WANG Hua-ming, LI Jia. Influence of heat treatments on microstructure and mechanical properties of laser additive manufacturing Ti−5Al−2Sn−2Zr−4Mo−4Cr titanium alloy [J]. Transactions of Nonferrous Metals Society of China,

2018, 28: 36−46. https://doi.org/10.1016/S1003-6326(18)64636-9.

[12] WANG Ke, WU Ming-yu, REN Zhao, ZHANG Yu, XIN Ren-long, LIU Qing. Static globularization and grain morphology evolution of α and β phases during annealing of hot-rolled TC21 titanium alloy [J]. Transactions of Nonferrous Metals Society of China, 2021, 31: 2664−2676. https://doi.org/10.1016/S1003-6326(21)65683-2.

[13] ELSHAER R N, IBRAHIM K M. Effect of cold deformation and heat treatment on microstructure and mechanical properties of TC21 Ti alloy [J]. Transactions of Nonferrous Metals Society of China, 2020, 30: 1290−1299. https://doi.org/10.1016/S1003-6326(20)65296-7.

[14] WU Chuan, ZHAN Mei. Effect of solution plus aging heat treatment on microstructural evolution and mechanical properties of near-β titanium alloy [J]. Transactions of Nonferrous Metals Society of China, 2019, 29: 997−1006. https://doi.org/10.1016/S1003-6326(19)65008-9.

[15] ZHENG Yun-fei, XU Li-juan, LIANG Zhen-quan, YU Jian-xin, WANG Xi-cheng, XIAO Shulong Xiao, XUE Xiang, TIAN Jing, CHEN Yu-yong. Investigation of three-step heat treatments on the microstructure and steady-state creep behaviors of (TiB+TiC+Y_2O_3)/α-Ti composite [J]. Materials Characterization, 2023, 204: 113181. https://doi.org/10.1016/j.matchar.2023.113181.

[16] SPIGARELLI S, PAOLETTI C, CERRI E, SANTACCHIA E, CABIBBO M. Creep response of Ti−6Al−4V alloy produced by additive manufacturing: Effect of annealing at 1050 °C [J]. Materials Science and Engineering A, 2022, 860: 144278. https://doi.org/10.1016/j.msea.2022.144278.

[17] KIM Y K, PARK S H, YU J H, ALMANGOUR B, LEE K A. Improvement in the high-temperature creep properties via heat treatment of Ti−6Al−4V alloy manufactured by selective laser melting [J]. Materials Science and Engineering A, 2018, 715: 33−40. https://doi.org/10.1016/j.msea.2017. 12.085.

[18] NIE Xian, LIU Hui-qun, ZHOU Xiao-zhou, YI Dan-qing, HUANG Bai-yun, HU Zhan, XU Yan-fei, YANG Qi, WANG Ding-chun, GAO Qi. Creep of Ti−5Al−5Mo−5V−1Fe−1Cr alloy with equiaxed and lamellar microstructures [J]. Materials Science and Engineering A, 2016, 651: 37−44. https://doi.org/10.1016/j.msea.2015.10.092.

[19] XIAO Li, TIAN Su-gui, BAO Xian-yu, CHEN Li-qing. Influence of heat treatment on microstructure and creep properties of hot continuous rolled Ti−6Al−4V alloy [J]. Materials Science and Engineering A, 2013, 559: 401−406. https://doi.org/10.1016/j.msea.2012.08.116.

[20] YU Ping-ju, HSU Yuan-yi, WANG Shing-hoa, YANG Jer-ren, YANG Yo-lun, CHANG Horng-yi, CHEN Chih-yuan, CHEN Hsueh-ren. Comparison of dynamic-aging creep and pre-aged creep in Ti-15-3 beta titanium alloy [J]. Materials Science and Engineering A, 2020, 798: 140135. https://doi. org/10.1016/j.msea.2020.140135.

[21] WANG Tong-bo, LI Bo-long Li, WANG Zhen-qiang, NIE Zuo-ren. A microstructure with improved thermal stability and creep resistance in a novel near-alpha titanium alloy [J]. Materials Science and Engineering A, 2018, 731: 12−20. https://doi.org/10.1016/j.msea.2018.06.034.

[22] CHEN Yu-yong, DU Zhao-xin, XIAO Shu-long, XU Li-juan, TIAN Jing. Effect of aging heat treatment on microstructure and tensile properties of a new β high strength titanium alloy [J]. Journal of Alloys and Compounds, 2014, 586: 588−592. https://doi.org/10.1016/j.jallcom.2013.10.096.

[23] DU Zhao-xin, XIAO Shu-long, XU Li-juan, TIAN Jing, KONG Fan-tao, CHEN Yu-yong. Effect of heat treatment on microstructure and mechanical properties of a new β high strength titanium alloy [J]. Materials & Design, 2014, 55: 183−190. https://doi.org/10.1016/j.matdes.2013.09.070.

[24] JONES N G, DASHWOOD R J, JACKSON M, DYE D. β Phase decomposition in Ti−5Al−5Mo−5V−3Cr [J]. Acta Materialia, 2009, 57(13): 3830−3839. https://doi.org/10.1016/j.actamat.2009.04.031.

[25] JULIEN D C T, BENOIT A, ELISABETH A G, SABINE D, GEORGES C, NADINE S. Transformation kinetics and microstructures of Ti17 titanium alloy during continuous cooling [J]. Materials Science and Engineering A, 2007, 448: 135−145. https://doi.org/10.1016/j.msea.2006.10. 024.

[26] ZHOU Wei, WANG Chang, LIU Ji-xiong, LI Si-yun, LIU Hui-qun. Aging precipitation sequence and effect of ω and secondary α phases on tensile properties of metastable β Ti−6Cr−5Mo−5V−4Al alloy [J]. Transactions of Nonferrous Metals Society of China, 2023, 33: 1742−1754. https://doi.org/10.1016/S1003-6326(23)66218-1.

[27] BIAN Ze-yu, ZHU Ai-lin, XIAO Ya-kai, LI Yu-gang, MA Nai-heng, BIAN Han-bing, WANG Ming-liang, CHEN Zhe, WANG Hao-wei. Coupling analysis on controlling mechanisms for creep of Al−Fe−Ni alloy [J]. Transactions of Nonferrous Metals Society of China, 2023, 33: 1331−1344. https://doi.org/10.1016/S1003-6326(23)66186-2.

[28] STINEHART J, PIZANO L F L P, XIONG W, ZHOU L. Creep property and microstructural evolution of laser powder bed fused binary Al−10Ce alloy [J]. Materials Science and Engineering A, 2023, 885: 145631. https://doi.org/10.1016/j.msea.2023.145631.

[29] ZONG Ying-ying, LIU Po, GUO Bin, SHAN De-bin. Investigation on high temperature short-term creep and stress relaxation of titanium alloy [J]. Materials Science and Engineering A, 2015, 620: 172−180. https://doi.org/10.1016/j.msea.2014.10.015.

[30] WANG Sheng-yuan, CHEN Li-jia, CHEN Xiao-Bo, ZHANG Hao-yu, ZHOU Ge. Effect of aging treatment on microstructure and tensile properties of Ti−4Al−6Mo−2V−5Cr−2Zr [J]. Journal of Materials Research and Technology, 2023, 22: 2008−2016. https://doi.org/10.1016/j.jmrt.2022.12.058.

[31] SAHOO R, JHA B B, SAHOO T K. Effect of microstructure on the creep properties of Ti−6Al−4V alloys: an analysis [J]. Transactions of the Indian Institute of Metals, 2018, 71(7): 1573−1582. https://doi.org/10.1007/s12666-018-1292-1.

[32] CHEN Zhao-qi, XU Li-juan, LIANG Zhen-quan, CAO Shou-zhen, YANG Jian-kai, XIAO Shu-long, TIAN Jing, CHEN Yu-yong. Effect of solution treatment and aging on microstructure, tensile properties and creep behavior of a hot-rolled β high strength titanium alloy with a composition of Ti−3.5Al−5Mo−6V−3Cr−2Sn−0.5Fe−0.1B−0.1C [J]. Materials Science and Engineering A, 2021, 823: 141728. https://doi.org/10.1016/j.msea.2021.141728.

[33] XIONG Y, KARAMCHED P, NGUYEN C, COLLINS D M, MAGAZZENI C M, TARLETON E, WILKINSON A J. Cold

creep of titanium: Analysis of stress relaxation using synchrotron diffraction and crystal plasticity simulations [J]. Acta Materialia, 2020, 199: 561−577. https://doi.org/10.1016/j.actamat.2020.08.010.

[34] ZHAO Qin-yang, BOLZONI L, CHEN Yong-nan, XU Yi-ku, TORRENS R, YANG Fei. Processing of metastable beta titanium alloy: Comprehensive study on deformation behavior and exceptional microstructure variation mechanisms [J]. Journal of Materials Science & Technology, 2022, 126: 22−43. https://doi.org/10.1016/j.jmst.2022.02.050.

[35] XIANG Wei, XIANG Yang, ZHANG Feng, FU Qiang, YUAN Wu-hua. Study on stress relaxation and creep behavior of TB18 titanium alloy during the aging process [J]. Materials Science and Engineering A, 2024, 893: 146125. https://doi.org/10.1016/j.msea.2024.146125.

热处理对 Ti−3.5Al−5Mo−6V−3Cr−2Sn−0.5Fe 高强 β 钛合金显微组织和蠕变性能的影响

杨建凯[1,2]，梁振泉[1,2]，肖树龙[1,2]，郑云飞[1,2]，王小松[1,2]，田 竟[1,2]，徐丽娟[1,2]

1. 哈尔滨工业大学 金属精密热加工国家级重点实验室，哈尔滨 150001；
2. 哈尔滨工业大学 材料科学与工程学院，哈尔滨 150001

摘 要：研究了热处理对 Ti−3.5Al−5Mo−6V−3Cr−2Sn−0.5Fe 高强 β 钛合金显微组织和蠕变性能的影响。结果表明，经 790 ℃固溶和时效处理(HT1)后，显微组织由等轴 α_p 相、β 相以及 α_s 相组成；经 840 ℃固溶和时效处理(HT2)后，显微组织由 β 相和 α_s 相组成。分析了 400 ℃时的蠕变行为，发现两种合金的应力指数均在 1~2 之间，扩散蠕变机制为主导蠕变机制之一。HT2 处理的合金抗蠕变性能更高。对 HT2 处理的合金进行 450 ℃、400 MPa 蠕变实验。结果表明，断裂机制为脆韧混合断裂。合金中相界面能够阻碍位错运动，同时，α_s 相能够与基体协调变形，从而减少了晶内裂纹的产生。

关键词：高强 β 钛合金；固溶和时效处理；蠕变行为；相析出；α_s 相粗化

(Edited by Bing YANG)